

Strong Evidence for ${}^9\text{N}$ and the Limits of Existence of Atomic Nuclei

R. J. Charity¹, J. Wylie^{2,3}, S. M. Wang^{4,5}, T. B. Webb⁶, K. W. Brown², G. Cerizza², Z. Chajecki⁷, J. M. Elson¹, J. Estee², D. E. M. Hoff^{1,*}, S. A. Kuvin^{8,†}, W. G. Lynch^{2,3}, J. Manfredi^{2,‡}, N. Michel⁹, D. G. McNeel^{8,†}, P. Morfouace^{1,2}, W. Nazarewicz^{2,3}, C. D. Pruitt¹, C. Santamaria², S. Sweany², J. Smith⁸, L. G. Sobotka^{1,6}, M. B. Tsang² and A. H. Wuosmaa⁸

¹Department of Chemistry, Washington University, St. Louis, Missouri 63130, USA

²Facility for Rare Isotope Beams, Michigan State University, East Lansing, Michigan 48824, USA

³Department of Physics and Astronomy, Michigan State University, East Lansing, Michigan 48824, USA

⁴Key Laboratory of Nuclear Physics and Ion-beam Application (MOE), Institute of Modern Physics, Fudan University, Shanghai 200433, China


⁵Shanghai Research Center for Theoretical Nuclear Physics, NSFC and Fudan University, Shanghai 200438, China

⁶Department of Physics, Washington University, St. Louis, Missouri 63130, USA

⁷Department of Physics, Western Michigan University, Kalamazoo, Michigan 49008, USA

⁸Department of Physics, University of Connecticut, Storrs, Connecticut 06269, USA

⁹Institute of Modern Physics, Chinese Academy of Sciences, Lanzhou 730000, China

 (Received 2 November 2022; revised 16 March 2023; accepted 7 September 2023; published 27 October 2023)

The boundaries of the chart of nuclides contain exotic isotopes that possess extreme proton-to-neutron asymmetries. Here we report on strong evidence of ${}^9\text{N}$, one of the most exotic proton-rich isotopes where more than one half of its constituent nucleons are unbound. With seven protons and two neutrons, this extremely proton-rich system would represent the first-known example of a ground-state five-proton emitter. The invariant-mass spectrum of its decay products can be fit with two peaks whose energies are consistent with the theoretical predictions of an open-quantum-system approach; however, we cannot rule out the possibility that only a single resonancelike peak is present in the spectrum.

DOI: [10.1103/PhysRevLett.131.172501](https://doi.org/10.1103/PhysRevLett.131.172501)

Nuclei with large imbalances between their constituent numbers of protons and neutrons can have exotic properties. The largest imbalances occur beyond the proton and neutron drip lines where the nuclear ground states (g.s.) are unbound. Because of the odd-even staggering of the drip lines induced by the nucleonic pairing, the shedding of unbound protons is usually terminated in an even- Z , particle-bound residue. Thus, just beyond the proton drip line, one is likely to find single-proton emitters for odd- Z isotopes and two-proton ($2p$) emitters for even- Z isotopes [1,2]. Even further removed, one finds $3p$ and $4p$ emitters. Presently, ${}^7\text{B}$, ${}^{13}\text{F}$, ${}^{17}\text{Na}$, and ${}^{31}\text{K}$ are the known $3p$ emitters [3–6] and ${}^8\text{C}$ and ${}^{18}\text{Mg}$ have been observed to decay by emission of four protons [7,8].

Moving outward past the drip lines, the decay widths of the low-lying states increase, eventually melting into an unresolvable continuum as their lifetimes become commensurate with typical reaction and single-particle timescales. Here, the very notion of the *nuclear state* becomes questionable as the timescales are too short to talk about the existence of a nucleus. Indeed, as discussed in Ref. [9], if a collection of nucleons survives for less than about 10^{-22} s, it should not be considered a nucleus. In this regime, the decay properties manifest themselves as *scattering features* rather than well-defined resonances. The maximum decay width at

the boundary for $A \approx 8$, based on single-particle timescales, is of order $\Gamma \approx 3.5$ MeV [10].

The $4p$ emitter ${}^8\text{C}$ has one half of its nucleons in the continuum and the remainder constitutes an α cluster. The nucleus ${}^9\text{N}$ is even more extreme with an additional proton in the continuum. In nuclei such as ${}^8\text{C}$ and ${}^9\text{N}$, we might anticipate difficulty in classifying nuclear properties in terms of localized nuclear states. On the other hand, new insights can be gained from such unbound clusters of nucleons. In this Letter, we make a careful distinction between *resonances* (sharp peaks in the experimental scattering cross section) and *resonant states* (complex-momentum poles of the scattering matrix). For the theoretical classification of resonant states, see Fig. 1. The decaying resonant states in the fourth quadrant of the complex- k plane, lying close to the real k axis and having a real energy $\text{Re}(E) > 0$ and a width $\Gamma = -2\text{Im}(E) > 0$, can be interpreted as narrow resonances seen in experiments. The poles with $\text{Re}(E) < 0$ and $\Gamma > 0$ can be associated with subthreshold resonant states ($\theta > 45^\circ$). The antibound states have $\text{Re}(E) < 0$ and $\Gamma = 0$.

Unlike the g.s. of ${}^8\text{C}$, the dineutron is not a genuine resonance (energy $E > 0$, decay width $\Gamma > 0$), but an antibound state (or a scattering feature) [11,12] located on the second Riemann energy sheet. Here the attractive interaction between the two neutrons is just insufficient

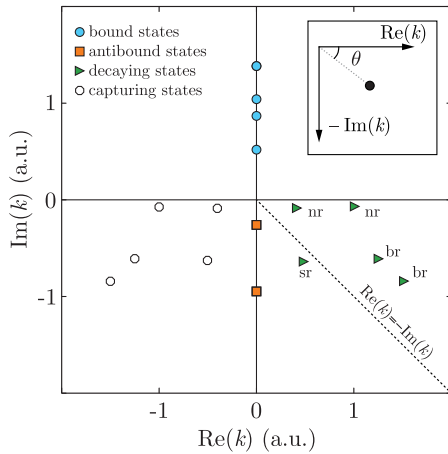


FIG. 1. Classification of resonant states based on the location of the scattering-matrix poles in the complex- k plane. The same arbitrary units (a.u.) are used on both axes. Bound, antibound, decaying, and capturing resonant states are marked, as well as narrow resonances (nr), broad resonant states (br), and subthreshold resonant states (sr). The distribution of poles is symmetric with respect to the imaginary k axis because of time reversal symmetry; thus, capturing states are presented as the time-reversed decaying states. The dashed -45° line separates decaying resonant states from subthreshold poles. The inset shows the polar angle θ of the resonant pole in the complex momentum plane.

to produce a bound state, but its nearly bound nature is manifested by enhanced $n+n$ scattering just above threshold and by strong final-state effects. The diproton is a subthreshold resonant state ($E < 0, \Gamma > 0$) [13,14] and located below the -45° line in the complex- k plane (see Fig. 1). It is formally neither an antibound state nor a resonance (though closer to the latter), and again manifests itself by enhanced scattering strength and final-state effects. While there have been some recent suggestions of a tetraneutron resonancelike structure, what was observed [15,16] may instead be a final-state effect [17,18]. Similar situations might occur in the g.s. of ${}^9\text{N}$ and ${}^9\text{He}$ as presented in this Letter.

The nucleus ${}^9\text{N}$ has three neutrons less than the lightest particle-bound nitrogen isotope ${}^{12}\text{N}$ and one more proton than ${}^8\text{C}$ into which it decays. The neighboring isotope ${}^{10}\text{N}$ has only been observed in three studies [19–21]. It has low-lying states which are single-proton resonances although their structure is not well established. Some indication as to the structure of ${}^9\text{N}$ can be gleaned from its mirror partner ${}^9\text{He}$ for which low-energy resonancelike states decay by the $n + {}^8\text{He}$ channel.

Particular interest in ${}^9\text{He}$ is due to the parity inversion of the ground-state spin for odd $N = 7$ isotones with large neutron excesses when the second $s_{1/2}$ neutron single-particle orbital intrudes into the p shell [22]. Most studies agree that there is a $1/2^-$ resonance around 1.2 MeV above the $n + {}^8\text{He}$ threshold (see Ref. [23]), but there is less agreement about its width [23–25]. A number of studies

find some $1/2^+$ strength below this resonance [23,25–28] although this strength in some studies is not sufficient to justify a notion of a state [25,28,29].

Experiment.—An $E/A = 69.5$ MeV secondary beam of ${}^{13}\text{O}$ (4×10^5 pps, purity 80%) was produced from the Coupled Cyclotron Facility at the National Superconducting Cyclotron Laboratory at Michigan State University. Charged particles created in the interaction with a 1-mm-thick ${}^9\text{Be}$ target were detected in the high resolution array (HiRA) [30] consisting of 14 $E - \Delta E$ telescopes covering scattering angles from 2.1° to 12.4° . The location of the HiRA telescopes was chosen based on Monte Carlo simulations which optimized the detection of low-lying resonances produced in projectile-fragmentation reactions. More details of the experiment and the simulations can be found in the Supplemental Material [31]. States in ${}^9\text{N}$ were produced in fragmentation reactions where three neutrons and one proton in total are removed from the projectile and the resonance is identified using the invariant-mass technique. Data from this experiment pertaining to the first observation of ${}^{11}\text{O}$ [49,50] and ${}^{13}\text{F}$ [4] as well as other previously known isotopes [21,51,52] have already been published.

Invariant-mass spectra.—The decay-energy (Q_{5p}) distribution for all detected $5p + \alpha$ events [Fig. 2(a)] is quite wide and contains no prominent “narrow” peaks, but there can be contributions from the decay of very wide ${}^9\text{N}$ states and nonresonant breakup. These events are produced in projectile-fragmentation reactions as their center-of-mass velocities are close to the beam value [53]. Given that the lowest-energy states in the mirror system ${}^9\text{He}$ decay to the $n + {}^8\text{He}(\text{g.s.})$ channel, it is thus interesting to look at the mirror $p + {}^8\text{C}(\text{g.s.})$ channel. For each $5p + \alpha$ event, we can remove one of the five protons in turn to create the five possible $4p + \alpha$ subevents. The distribution of ${}^8\text{C}$ decay energy (Q_{4p}) from these subevents [Fig. 2(b)] has a peak corresponding to the g.s. of ${}^8\text{C}$ at the expected value of Q_{4p} . For comparison, the dotted green curve shows the shape of the ${}^8\text{C}$ peak obtained from fitting the more numerous $4p + \alpha$ events (see Supplemental Material [31]).

Possible ${}^9\text{N} \rightarrow p + {}^8\text{C}(\text{g.s.})$ decay events were selected by requiring that at least one of the $4p + \alpha$ subevents lies in the gate around the ground-state peak [Fig. 2(b)]. Based on the presented fit to the ground-state peak in this figure, 20% of the $4p + \alpha$ subevents in this gate are associated with the background component. However, the gate on $p + {}^8\text{C}(\text{g.s.})$ is cleaner than this as some of the events contribute to both the peak and this background through their different subevents. Indeed, 11% of selected events have two subevents in this gate which accounts for 1/2 of the background contamination. These numerical partitions are confirmed by our simulations.

The final distribution, with the ${}^8\text{C}(\text{g.s.})$ gate, is largely restricted to $Q_{5p} < 10$ MeV [data points Fig. 2(a)] and

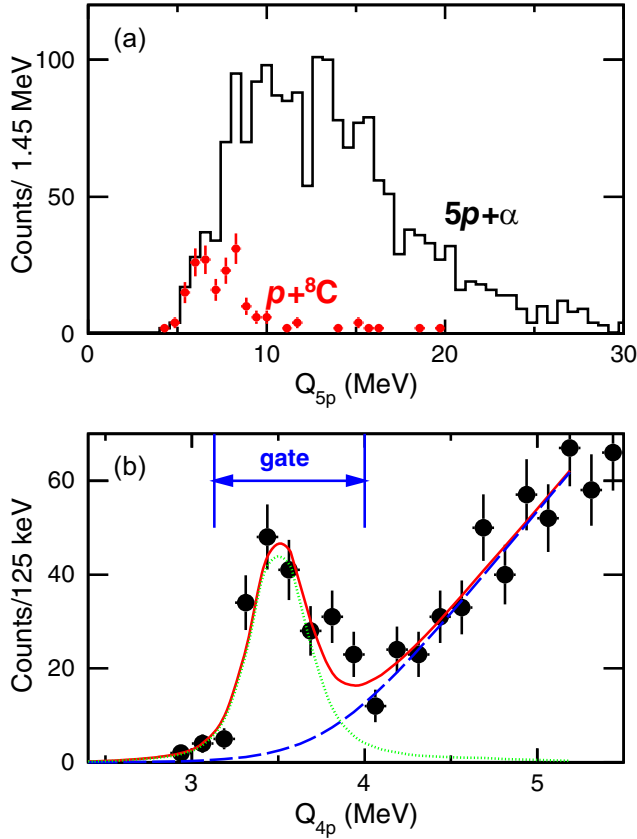


FIG. 2. Invariant-mass spectra for ${}^9\text{N}$ and ${}^8\text{C}$. (a) Histogram shows the distribution of the decay energy Q_{5p} obtained from $5p + \alpha$ events with the invariant-mass method. The data points show the distribution where an ${}^8\text{C}(\text{g.s.})$ intermediate state was identified. (b) The data points show the distribution of ${}^8\text{C}$ decay energy (Q_{4p}) from the five $4p + \alpha$ subevents in each $5p + \alpha$ event. The solid red curve shows a fit to this distribution using the experimental ${}^8\text{C}$ line shape obtained from detected $4p + \alpha$ events (dotted green curve) plus a smooth background (dashed blue curve). The gate used to select $p + {}^8\text{C}(\text{g.s.})$ events is indicated.

appears to have two peaks. Hence it may be a doublet rather than a singlet although the statistics are marginal for this distinction.

Theoretical models.—Since continuum effects are strong for both ${}^8\text{C}$ and ${}^9\text{N}$, we used the complex-energy Gamow shell model (GSM) to predict the location of the nuclear states of interest as it has been used to study many weakly bound and unbound systems [54–56] including the g.s. of ${}^8\text{C}$ [32]. GSM differs from the traditional closed-quantum-system nuclear shell model as it allows for bound, scattering, and Gamow resonant states with outgoing asymptotic behavior to be treated on equal footing by implementing the Berggren basis [57].

Calculations for ${}^8\text{C}$ and ${}^9\text{N}$ were performed by assuming an α core surrounded by four and five valence protons, respectively. We used the same valence-space Hamiltonian as described in previous GSM studies [32,33,58] with the

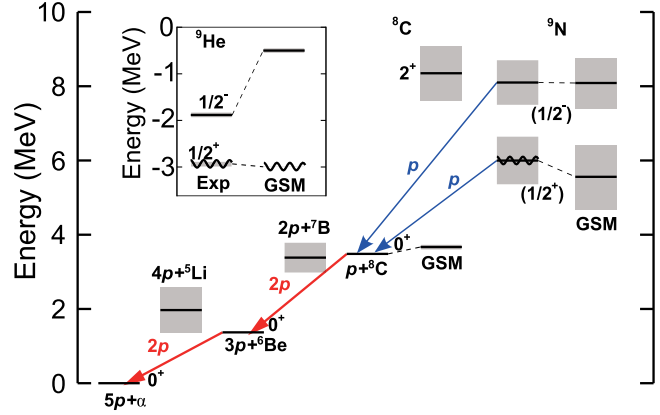


FIG. 3. Level diagrams of ${}^8\text{C}$ and ${}^9\text{N}$ obtained experimentally and calculated with the GSM. Energies are given relative to the ${}^4\text{He}$ threshold. The level diagram of ${}^9\text{He}$, the mirror partner of ${}^9\text{N}$, is shown in the inset. The $1/2^+$ antibound state in ${}^9\text{He}$ is shown with a wavy line to indicate its status more as a scattering feature rather than a real state. The proposed $1/2^+$ state in ${}^9\text{N}$ is shown with both straight and wavy lines to indicate the uncertainty as to its nature (a resonance or scattering feature) while the GSM interprets it as a broad resonant state.

parameters given in the Supplemental Material [31]. The maximum number of particles allowed in the continuum is 2 for the results presented; it has been checked that more particles in the continuum barely change the conclusion for the $A = 8$ system. The predicted Q_{4p} values for the g.s. and the 2^+ first excited state of ${}^8\text{C}$ shown in Fig. 3 with the relevant levels for their decay are around 3.7 and 8.3 MeV, respectively (see Supplemental Material [31]; see also Ref. [59] for complex-scaling predictions of ${}^8\text{C}$).

The properties of the low-lying states in ${}^9\text{N}$ were cross-checked by the Gamow-coupled-channel (GCC) method [34,60], which is a complex framework utilizing the Berggren basis. Based on large proton-decaying spectroscopic factors ($S_{s_{1/2}}^2 = 0.87$ and $S_{p_{1/2}}^2 = 0.80$ according to GSM calculations), ${}^9\text{N}$ can be described as a ${}^8\text{C} + p$ two-body system.

Discussion.—While we have cleanly selected $p + {}^8\text{C}(\text{g.s.})$ events, the extra proton beyond the ${}^8\text{C}$ decay products can result from either ${}^9\text{N}$ resonant decay or alternatively is produced directly in the first step of the projectile-fragmentation reaction. To form ${}^9\text{N}$, one proton and three neutrons need to be removed from the projectile and thus one prompt proton would be expected unless it is bound in a d or t cluster with some of the promptly removed neutrons. Also, there can be contributions from events where the projectile promptly breaks up into the channel $2p + 3n + {}^8\text{C}(\text{g.s.})$. While most of the promptly emitted protons are expected at larger angles than sampled with HiRA, we do expect some background from these prompt particles [53].

The background from all these sources of prompt protons has been extensively studied in Ref. [53] for this and other resonant-decay channels associated with this projectile. The Q_{5p} dependence of this background can be obtained from mixing p and ${}^8\text{C}(\text{g.s.})$ decay products from different $p + {}^8\text{C}(\text{g.s.})$ events appropriately weighted to include correlations between them. However, this predicted Q_{5p} distribution is too wide to explain all the observed events and thus substantial contributions from ${}^9\text{N}$ resonances are required [53]. Indeed, the possibility that statistical fluctuations in this background can explain the observed spectrum can be ruled out with a significance of roughly 5σ , i.e., at the discovery threshold for a new resonance (see Supplemental Material [31]).

The GSM predicts $1/2^+$ and $1/2^-$ states in the region below $Q_{5p} = 10$ MeV where the $p + {}^8\text{C}(\text{g.s.})$ yield is strongest. The predicted ground state has the same parity inversion as observed for ${}^{11}\text{Be}$ [22]. With two states and the magnitude of the background to vary, there are seven fit parameters, which is about the same as the number of data points in the peak region. Thus the experimental statistics are presently not sufficient to fully constrain the location of both resonance poles ($Q_{1p} - i\Gamma/2$) and determined their nature (genuine or subthreshold resonances) from Fig. 1. In the following, in order to show some possible interpretations of the data, we present some constrained fits which avoid overfitting.

At one extreme, we can assume just a single peak plus background. Using R -matrix line shapes [35] for the $p + {}^8\text{C}(\text{g.s.})$ channel, the qualities of the fits were very similar for both s and p resonances. The resonance pole for a single s -wave fit is at $Q_{1p} = 1.22(16)$ MeV [$Q_{5p} = 4.70(16)$] and $\Gamma = 2.59(23)$ MeV. Such a state is approaching the diffuse borderland between a broad resonance and a scattering feature. However, this solution is disfavored as the magnitude of the background has been reduced to zero to achieve the best fit. The result is not much better for a single p -wave resonance [Fig. 4(a)] with the resonance pole given by $Q_{1p} = 2.01(16)$ MeV [$Q_{5p} = 5.49(16)$] and $\Gamma = 2.28(23)$ MeV. In this case, the fitted background (dashed blue curve) contributes only 14% of the total yield. As other resonant channels from this ${}^{13}\text{O}$ -induced reaction had backgrounds of magnitude 30%–54% [53], these single-peak solutions are disfavored.

Figure 4(b) shows an example of a possible two-peak fit assuming real $p + {}^8\text{C}(\text{g.s.})$ resonances described by R -matrix line shapes. Here, the R -matrix parameters of the $1/2^-$ peak are fixed so that its pole is consistent with the GSM prediction. With this constraint, the fitted values for the $1/2^+$ strength are $Q_{1p} = 2.75(21)$ MeV [$Q_{5p} = 6.23(21)$] and $\Gamma = 0.58(44)$ MeV, which can be compared to the GSM predictions of $Q_{5p} = 5.56$ MeV and $\Gamma = 1.74$ MeV. The fitted background from prompt protons (dashed blue curve) now explains the observed

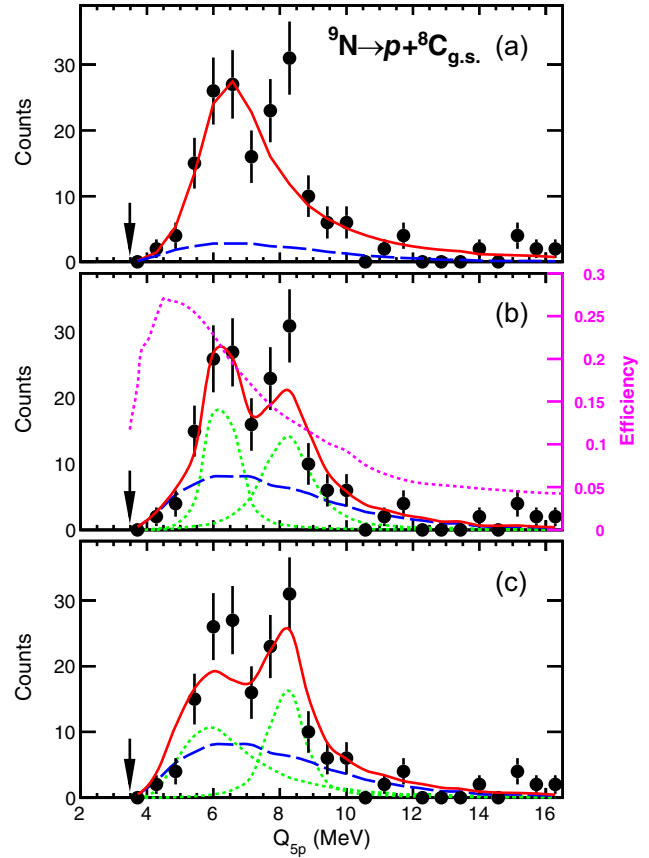


FIG. 4. Fits (solid red curves) to the selected $p + {}^8\text{C}(\text{g.s.})$ distribution. (a) Fit with a single peak parametrized by an $\ell = 1$ R -matrix line shape. (b),(c) Two peak fits where the contributions from both levels are given by the dotted green curves. The fit in (b) was using a $p + {}^8\text{C}(\text{g.s.})$ R -matrix line shape where energy and width of the upper peak are set to the GSM predictions for the $J^\pi = 1/2^-$ state of ${}^9\text{N}$. The dependence of the detection efficiency as a function of Q_{5p} as determined in our Monte Carlo simulations (see Supplemental Material [31]) is shown by the dashed magenta curve. The fit in (c) was obtained where the fixed width of the $1/2^-$ was halved from its value in (b) and the $1/2^+$ strength is described by a subthreshold resonant state using GCC line shape. In all panels, the $p + {}^8\text{C}(\text{g.s.})$ threshold is indicated by an arrow and the fitted background from nonresonant protons is shown by the dashed blue curves.

yields below $Q_{5p} = 5$ MeV and the high-energy tail above 10 MeV. This background accounts for $\approx 40\%$ of the yield, which is similar to values of 30%–54% obtained in fitting the ${}^{10,11}\text{N} \rightarrow p + {}^{9,10}\text{C}$ invariant-mass distributions [53]. While this fitted width of the $1/2^+$ state is smaller than the GSM prediction, it can be increased by decreasing the fixed width of the $1/2^-$ state. For example, Fig. 4(c) shows a fit where the intrinsic width of the $1/2^-$ state has been halved, but now the $1/2^+$ strength is described by the GCC line shape as a subthreshold resonant state.

To provide insights into the nature of the $1/2^+$ state in ${}^9\text{N}$, GSM calculations were performed for its mirror partner,

${}^9\text{He}$, using the same Hamiltonian parameters. Figure 3 shows that the experimental spectrum is reasonably reproduced, although the prediction for the $1/2^-$ state is somewhat too high in energy. The previous studies using the Berggren basis have indicated that the $1/2^+$ state in ${}^9\text{He}$ is a resonance [33,36], in which some bound poles were introduced in the basis to stabilize their results (see Supplemental Material for details [31]). However, when the continuum effect is properly taken into account in the current work with a deformed scattering contour [37], one can generate an antibound $1/2^+$ pole in ${}^9\text{He}$, an approach yielding the best agreement with experimental data.

Although it is not possible for antibound poles to emerge in proton-rich nuclei due to the Coulomb interaction [34], we followed the same procedure as in ${}^9\text{He}$ to determine if the $1/2^+$ state in ${}^9\text{N}$ is a broad resonant state or subthreshold resonant state. The predicted $1/2^+$ state has an energy of $E = 2.08$ MeV above the ${}^8\text{C} + p$ threshold and $\Gamma = 1.74$ MeV, which indicates a broad resonant state as defined in Fig. 1. It must be noted, however, that the $1/2^+$ state in GSM is very fragile with respect to changes of the Berggren basis due to the truncations (particle-hole, discretization of the continuum) employed (see Supplemental Material for details [31]), so we cannot with certainty rule out a subthreshold resonant state.

Both ${}^8\text{C}$ and ${}^9\text{N}$ shed their excess protons by sequential steps of either single-proton or prompt $2p$ decays. The $4p$ -emitter ${}^{18}\text{Mg}$ also decays in this manner [8], suggesting this behavior is typical for isotopes at the limits of existence. Our analysis suggests that some observed structures, sometimes interpreted in terms of nuclear states, should be viewed rather as fleeting features lying outside the chart of nuclides.

Conclusions.—We have found strong evidence for the exotic nuclide ${}^9\text{N}$ produced in the fragmentation of a ${}^{13}\text{O}$ beam. The invariant-mass spectrum of detected $5p + \alpha$ events, each containing an ${}^8\text{C}(\text{g.s.})$ intermediate state, contains a structure which cannot be explained at the $\approx 5\sigma$ level by statistical fluctuations of the expected background from other coincident protons liberated in the fragmentation event. This observed structure can be interpreted as two ${}^9\text{N}$ peaks, although a single-peak solution cannot be totally discounted. The ${}^9\text{N}$ state(s) would be first-known case(s) of $5p$ emission from ground-state and low-lying resonances.

This nuclide has also been studied theoretically in the Gamow shell model where the important effects of the continuum are included. The predicted locations of the $1/2^+$ and $1/2^-$ resonant states are in excellent agreement with the location of the observed structure giving further evidence for the preferred two-peak solution. In the model, the $1/2^+$ ground state of ${}^9\text{N}$ is the mirror of an antibound state in ${}^9\text{He}$, and is most likely a broad resonant state rather

than a subthreshold resonant state. However, the latter cannot be completely ruled out in both the experiment and the theory.

This material is based upon work supported by the U.S. Department of Energy, Office of Science, Office of Nuclear Physics under Awards No. DE-FG02-87ER-40316, No. DE-FG02-04ER-41320, No. DE-SC0014552, No. DOE-DE-SC0013365, No. DE-SC0023175, the National Science Foundation under Grant No. PHY-156556, the National Key Research and Development Program (MOST 2022YFA1602303), and the National Natural Science Foundation of China under Grants No. 12175281 and No. 12147101. J.M. was supported by a Department of Energy National Nuclear Security Administration Steward Science Graduate Fellowship under Cooperative Agreement No. DE-NA0002135.

*Present address: Lawrence Livermore National Laboratory, Livermore, California 94550, USA.

†Present address: Los Alamos National Laboratory, Los Alamos, New Mexico 87545, USA.

‡Present address: Department of Engineering Physics, Air Force Institute of Technology, Wright-Patterson AFB, Ohio 45433, USA.

- [1] M. Pfützner, M. Karny, L. V. Grigorenko, and K. Riisager, Radioactive decays at limits of nuclear stability, *Rev. Mod. Phys.* **84**, 567 (2012).
- [2] L. Neufcourt, Y. Cao, S. Giuliani, W. Nazarewicz, E. Olsen, and O. B. Tarasov, Beyond the proton drip line: Bayesian analysis of proton-emitting nuclei, *Phys. Rev. C* **101**, 014319 (2020).
- [3] R. J. Charity *et al.*, Investigations of three-, four-, and five-particle decay channels of levels in light nuclei created using a ${}^9\text{C}$ beam, *Phys. Rev. C* **84**, 014320 (2011).
- [4] R. J. Charity *et al.*, Observation of the Exotic Isotope ${}^{13}\text{F}$ Located Four Neutrons Beyond the Proton Drip Line, *Phys. Rev. Lett.* **126**, 132501 (2021).
- [5] K. W. Brown, R. J. Charity, J. M. Elson, W. Reviol, L. G. Sobotka, W. W. Buhro, Z. Chajecski, W. G. Lynch, J. Manfredi, R. Shane, R. H. Showalter, M. B. Tsang, D. Weisshaar, J. R. Winkelbauer, S. Bedoor, and A. H. Wuosmaa, Proton-decaying states in light nuclei and the first observation of ${}^{17}\text{Na}$, *Phys. Rev. C* **95**, 044326 (2017).
- [6] D. Kostyleva *et al.*, Towards the Limits of Existence of Nuclear Structure: Observation and First Spectroscopy of the Isotope ${}^{31}\text{K}$ by Measuring its Three-Proton Decay, *Phys. Rev. Lett.* **123**, 092502 (2019).
- [7] R. J. Charity *et al.*, $2p - 2p$ decay of ${}^8\text{C}$ and isospin-allowed $2p$ decay of the isobaric-analog state in ${}^8\text{B}$, *Phys. Rev. C* **82**, 041304(R) (2010).
- [8] Y. Jin *et al.*, First Observation of the Four-Proton Unbound Nucleus ${}^{18}\text{Mg}$, *Phys. Rev. Lett.* **127**, 262502 (2021).
- [9] M. Thoennessen, Reaching the limits of nuclear stability, *Rep. Prog. Phys.* **67**, 1187 (2004).

- [10] K. Fosse, W. Nazarewicz, Y. Jaganathen, N. Michel, and M. Płoszajczak, Nuclear rotation in the continuum, *Phys. Rev. C* **93**, 011305(R) (2016).
- [11] H. C. Ohanian and C. G. Ginsburg, Antibound 'states' and resonances, *Am. J. Phys.* **42**, 310 (1974).
- [12] V. A. Babenko and N. M. Petrov, Low-energy parameters of neutron-neutron interaction in the effective-range approximation, *Phys. At. Nucl.* **76**, 684 (2013).
- [13] L. P. Kok, Accurate Determination of the Ground-State Level of the ${}^2\text{He}$ Nucleus, *Phys. Rev. Lett.* **45**, 427 (1980).
- [14] A. M. Mukhamedzhanov, B. F. Irgaziev, V. Z. Goldberg, Y. V. Orlov, and I. Qazi, Bound, virtual, and resonance S -matrix poles from the Schrödinger equation, *Phys. Rev. C* **81**, 054314 (2010).
- [15] K. Kisamori *et al.*, Candidate Resonant Tetraneutron State Populated by the ${}^4\text{He}({}^8\text{He}, {}^8\text{Be})$ Reaction, *Phys. Rev. Lett.* **116**, 052501 (2016).
- [16] M. Duer *et al.*, Observation of a correlated free four-neutron system, *Nature (London)* **606**, 678 (2022).
- [17] A. Deltuva, Tetraneutron: Rigorous continuum calculation, *Phys. Lett. B* **782**, 238 (2018).
- [18] M. D. Higgins, C. H. Greene, A. Kievsky, and M. Viviani, Nonresonant Density of States Enhancement at Low Energies for Three or Four Neutrons, *Phys. Rev. Lett.* **125**, 052501 (2020).
- [19] A. Lépine-Szily, J. M. Oliveira, V. R. Vanin, A. N. Ostrowski, R. Lichtenthäler, A. Di Pietro, V. Guimarães, A. M. Laird, L. Maunoury, G. F. Lima, F. de Oliveira Santos, P. Roussel-Chomaz, H. Savajols, W. Trinder, A. C. C. Villari, and A. de Vismes, Observation of the particle-unstable nucleus ${}^{10}\text{N}$, *Phys. Rev. C* **65**, 054318 (2002).
- [20] J. Hooker, G. Rogachev, V. Goldberg, E. Koshchiy, B. Roeder, H. Jayatissa, C. Hunt, C. Magana, S. Upadhyayula, E. Uberseder, and A. Saastamoinen, Structure of ${}^{10}\text{N}$ in ${}^9\text{C} + p$ resonance scattering, *Phys. Lett. B* **769**, 62 (2017).
- [21] R. J. Charity, T. B. Webb, L. G. Sobotka, and K. W. Brown, Spectroscopy of ${}^{10}\text{N}$ with the invariant-mass method, *Phys. Rev. C* **104**, 054307 (2021).
- [22] T. Aumann *et al.*, One-Neutron Knockout from Individual Single-Particle States of ${}^{11}\text{Be}$, *Phys. Rev. Lett.* **84**, 35 (2000).
- [23] T. Al Kalanee *et al.*, Structure of unbound neutron-rich ${}^9\text{He}$ studied using single-neutron transfer, *Phys. Rev. C* **88**, 034301 (2013).
- [24] H. G. Bohlen, B. Gebauer, D. Kolbert, W. von Oertzen, E. Stiliaris, M. Wilpert, and T. Wilpert, Spectroscopy of ${}^9\text{He}$ with the (${}^{13}\text{C}$, ${}^{13}\text{O}$)-reaction on ${}^9\text{Be}$, *Z. Phys. A* **330**, 227 (1988).
- [25] D. Votaw *et al.*, Low-lying level structure of the neutron-unbound $N = 7$ isotones, *Phys. Rev. C* **102**, 014325 (2020).
- [26] L. Chen, B. Blank, B. Brown, M. Chartier, A. Galonsky, P. Hansen, and M. Thoennessen, Evidence for an $l = 0$ ground state in ${}^9\text{He}$, *Phys. Lett. B* **505**, 21 (2001).
- [27] M. S. Golovkov *et al.*, New insight into the low-energy ${}^9\text{He}$ spectrum, *Phys. Rev. C* **76**, 021605(R) (2007).
- [28] H. Johansson *et al.*, The unbound isotopes ${}^9, {}^{10}\text{He}$, *Nucl. Phys. A* **842**, 15 (2010).
- [29] M. Vorabbi, A. Calci, P. Navrátil, M. K. G. Kruse, S. Quaglioni, and G. Hupin, Structure of the exotic ${}^9\text{He}$ nucleus from the no-core shell model with continuum, *Phys. Rev. C* **97**, 034314 (2018).
- [30] M. Wallace *et al.*, The high resolution array (HiRA) for rare isotope beam experiments, *Nucl. Instrum. Methods Phys. Res., Sect. A* **583**, 302 (2007).
- [31] See Supplemental Material at <http://link.aps.org/supplemental/10.1103/PhysRevLett.131.172501> for more details on beam production, experimental apparatus, Monte Carlo simulations, analysis of background fluctuations, theory calculations, and the list of the predicted states, which includes Refs. [3,7,23,32–48].
- [32] J. Wylie, J. Okołowicz, W. Nazarewicz, M. Płoszajczak, S. M. Wang, X. Mao, and N. Michel, Spectroscopic factors in dripline nuclei, *Phys. Rev. C* **104**, L061301 (2021).
- [33] Y. Jaganathen, R. M. Id Betan, N. Michel, W. Nazarewicz, and M. Płoszajczak, Quantified Gamow shell model interaction for psd -shell nuclei, *Phys. Rev. C* **96**, 054316 (2017).
- [34] S. M. Wang, W. Nazarewicz, R. J. Charity, and L. G. Sobotka, Structure and decay of the extremely proton-rich nuclei ${}^{11,12}\text{O}$, *Phys. Rev. C* **99**, 054302 (2019).
- [35] A. M. Lane and R. G. Thomas, R -matrix theory of nuclear reactions, *Rev. Mod. Phys.* **30**, 257 (1958).
- [36] K. Fosse, J. Rotureau, and W. Nazarewicz, Energy spectrum of neutron-rich helium isotopes: Complex made simple, *Phys. Rev. C* **98**, 061302(R) (2018).
- [37] N. Michel, W. Nazarewicz, M. Płoszajczak, and J. Rotureau, Antibound states and halo formation in the Gamow shell model, *Phys. Rev. C* **74**, 054305 (2006).
- [38] D. Bazin, V. Andreev, A. Becerril, M. Doléans, P. Mantica, J. Ottarson, H. Schatz, J. Stoker, and J. Vincent, Radio frequency fragment separator at NSCL, *Nucl. Instrum. Methods Phys. Res., Sect. A* **606**, 314 (2009).
- [39] R. J. Charity, K. W. Brown, J. Elson, W. Reviol, L. G. Sobotka, W. W. Buhro, Z. Chajecki, W. G. Lynch, J. Manfredi, R. Shane, R. H. Showalter, M. B. Tsang, D. Weisshaar, J. Winkelbauer, S. Bedoor, D. G. McNeel, and A. H. Wuosmaa, Invariant-mass spectroscopy of ${}^{18}\text{Ne}$, ${}^{16}\text{O}$, and ${}^{10}\text{C}$ excited states formed in neutron-transfer reactions, *Phys. Rev. C* **99**, 044304 (2019).
- [40] K. W. Brown, W. W. Buhro, R. J. Charity, J. M. Elson, W. Reviol, L. G. Sobotka, Z. Chajecki, W. G. Lynch, J. Manfredi, R. Shane, R. H. Showalter, M. B. Tsang, D. Weisshaar, J. R. Winkelbauer, S. Bedoor, and A. H. Wuosmaa, Two-proton decay from the isobaric analog state in ${}^8\text{B}$, *Phys. Rev. C* **90**, 027304 (2014).
- [41] I. A. Egorova *et al.*, Democratic Decay of ${}^6\text{Be}$ Exposed by Correlations, *Phys. Rev. Lett.* **109**, 202502 (2012).
- [42] Evaluated Nuclear Structure Data File (ENSDF), <http://www.nndc.bnl.gov/ensdf>.
- [43] G. Cowan, *Statistical Data Analysis* (Clarendon Press, Oxford, 1998).
- [44] W. A. Rolke and A. M. López, How to claim a discovery, <https://www.slac.stanford.edu/econf/C030908/papers/MOBT002.pdf>.
- [45] P. K. Sinervo, Signal significance in particle physics, [arXiv: hep-ex/0208005](https://arxiv.org/abs/hep-ex/0208005).

- [46] G. Aad *et al.* (ATLAS Collaboration), Observation of a new particle in the search for the standard model Higgs boson with the ATLAS detector at the LHC, *Phys. Lett. B* **716**, 1 (2012).
- [47] S. Chatrchyan *et al.* (CMS Collaboration), Observation of a new boson at a mass of 125 GeV with the CMS experiment at the LHC, *Phys. Lett. B* **716**, 30 (2012).
- [48] L. Lyons, Discovering the significance of 5σ , [arXiv:1310.1284](https://arxiv.org/abs/1310.1284).
- [49] T. B. Webb *et al.*, Particle decays of levels in $^{11,12}\text{N}$ and ^{12}O investigated with the invariant-mass method, *Phys. Rev. C* **100**, 024306 (2019).
- [50] T. B. Webb *et al.*, Invariant-mass spectrum of ^{11}O , *Phys. Rev. C* **101**, 044317 (2020).
- [51] T. B. Webb *et al.*, First Observation of Unbound ^{11}O , the Mirror of the Halo Nucleus ^{11}Li , *Phys. Rev. Lett.* **122**, 122501 (2019).
- [52] R. J. Charity *et al.*, Using spin alignment of inelastically excited nuclei in fast beams to assign spins: The spectroscopy of ^{13}O as a test case, *Phys. Rev. C* **104**, 024325 (2021).
- [53] R. J. Charity and L. G. Sobotka, companion paper, Invariant-mass spectroscopy in projectile-fragmentation reactions, *Phys. Rev. C* **108**, 044318 (2023).
- [54] N. Michel, W. Nazarewicz, M. Płoszajczak, and K. Bennaceur, Gamow Shell Model Description of Neutron-Rich Nuclei, *Phys. Rev. Lett.* **89**, 042502 (2002).
- [55] N. Michel, W. Nazarewicz, M. Płoszajczak, and T. Vertse, Shell model in the complex energy plane, *J. Phys. G* **36**, 40 (2009).
- [56] N. Michel and M. Płoszajczak, *Gamow Shell Model, The Unified Theory of Nuclear Structure and Reactions*, Lecture Notes in Physics Vol. 983 (Springer, Cham, Switzerland, 2021).
- [57] T. Berggren, On the use of resonant states in eigenfunction expansions of scattering and reaction amplitudes, *Nucl. Phys. A* **109**, 265 (1968).
- [58] X. Mao, J. Rotureau, W. Nazarewicz, N. Michel, R. M. Id Betan, and Y. Jaganathen, Gamow-shell-model description of Li isotopes and their mirror partners, *Phys. Rev. C* **102**, 024309 (2020).
- [59] T. Myo, M. Odsuren, and K. Katō, Five-body resonances in ^8He and ^8C using the complex scaling method, *Phys. Rev. C* **104**, 044306 (2021).
- [60] S. M. Wang and W. Nazarewicz, Fermion Pair Dynamics in Open Quantum Systems, *Phys. Rev. Lett.* **126**, 142501 (2021).